Liquid Crystals
Publication details, including instructions for authors and subscription information:
http://www.informaworld.com/smpp/title~content=t713926090

Two-dimensional Monte Carlo studies of lipid molecules in a bilayer membrane

D. P. Fraser[a]; R. W. Chantrell[a]; D. Melville[a]; D. J. Tildesley[b]
[a] School of Physics and Astronomy, Lancashire Polytechnic, Preston, England [b] Department of Chemistry, The University, Southampton, England

To cite this Article Fraser, D. P. , Chantrell, R. W. , Melville, D. and Tildesley, D. J.(1988) 'Two-dimensional Monte Carlo studies of lipid molecules in a bilayer membrane', Liquid Crystals, 3: 4, 423 — 441
To link to this Article: DOI: 10.1080/02678298808086392
URL: http://dx.doi.org/10.1080/02678298808086392

LIQUID CRYSTALS, 1988, VOL. 3, NO. 4, 423–441

Two-dimensional Monte Carlo studies of lipid molecules in a bilayer membrane

by D. P. FRASER, R. W. CHANTRELL and D. MELVILLE
School of Physics and Astronomy, Lancashire Polytechnic, Preston PR1 2TQ, England
and D. J. TILDESLEY
Department of Chemistry, The University, Southampton SO9 5NH, England

(*Received 29 September 1987; accepted 16 December 1987*)

We present a new model to study in-plane liquid properties of lipid membranes. The different conformations of lipids are represented by a seven-state system of hard triatomic particles, or triples, of varying lengths which correspond to the different cross-sectional areas of the lipids in the plane of the membrane. Two-dimensional Monte Carlo simulations are performed in both the constant NVT and NPT ensembles. The distribution of states has a strong density dependence and a small temperature dependence over the biologically relevant range. There is no long range orientational order in the systems before freezing. The short range orientational order increases with density. Widom's particle insertion method is used to obtain the excess chemical potential of the system for the seven states. These values, along with the pressure, are in excellent agreement with estimates from scaled particle theory.

1. Introduction

Biological membranes can be approximated using simple models appropriate to liquid-crystalline structure [1]. The basic lipid bilayer can be modelled as a single sheet of one of the lamellar phases. At low temperatures there is some long range translational order of the chains although in the gel phase the head groups are not translationally ordered. Most of the lipid hydrocarbon chains are in the all-trans state, although there are a small number of g^+tg^- kinks in the gel phase. Co-operative tilting of the layers can occur [2]. As the temperature increases the bilayer exhibits ripple phases with the chains still translationally ordered [3]. At the liquid-condensed to liquid-expanded phase transition the translational order of the chains disappears and the number of gauche rotations increases giving rise to many different chain conformers. The molecules are, however, still preferentially oriented normal to the bilayer [4]. A detailed understanding of the structure of these phases and the nature of the phase transitions is the key to understanding transport of ions through the bilayer [5].

Most previous modelling of lipid bilayers has been aimed at understanding phase transitions [6–14], or the orientational ordering of the hydrocarbon chains [15–19]. In this paper we study the structure and conformational order in the liquid phase of a simple model of the bilayer. Our model is in the spirit of that studied by Werge and Binder [20] who used molecular dynamics (MD) and Monte Carlo (MC) to study Lennard-Jones diatomic molecules in two dimensions. The diatomics represented the

projections of the all-trans phospholipids on to the plane of the head group but the simulations took no account of any conformational changes in the phospholipids and hence their two-dimensional projections. The work presented here models the lipids as projections on to the plane of the head groups, but takes into account conformational changes in the underlying lipid, using the approach of Scott [10] and Scott and Cheng [7]. This study assumes that the structure determining interaction in the lipid bilayer is the excluded volume of the conformationally disordered chains. The lipid–lipid interaction is a hard core repulsion. This can easily be supplemented with attractive interactions such as the dispersion between chains and any electrostatic interactions between the head groups in future studies.

Although only lipids are included in our model, it would also be possible to include proteins by introducing much larger hard discs into the two-dimensional analogue.

The aim of this work is not to build a realistic model for the bilayer but to gain some understanding of the role of volume exclusion in determining the in-plane liquid structure in these systems. It is not our aim to describe the chain-melting transition in detail.

In §2 we describe the model; §3 outlines the simulation and in §4 we discuss our results.

2. The model

The starting point for this simulation is the fluid mosaic model of Singer and Nicolson [21] which is shown in figure 1. The high mobility of the lipid molecules [22] suggests that the chains do not tend to become entangled with neighbouring lipids. The molecules can thus be represented approximately by cylinders for which the end planes correspond to the projections of the cross-sectional areas of the molecules on to the plane of the membrane. If it is assumed that there is little or no interaction between the lipids in the two halves of the bilayer then the membrane can be represented simply by this two-dimensional projection of the molecules. The many different conformers are classified and described by Scott and Cheng [7]. The result is a system of chain states, each of which has an associated degeneracy, ω_i, a hard core area per molecule, A_i, and an average number of gauche rotations, g_i. The number of states depends upon the lipid molecule under consideration. For this work, the seven-state model for dipalmitoylphosphatidylcholine (DPPC) has been used. In one

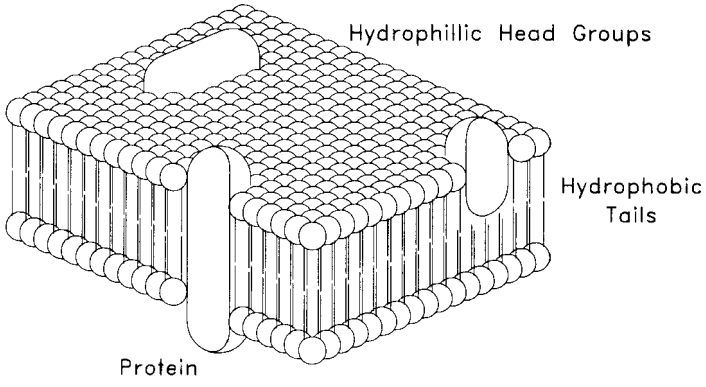

Figure 1. The fluid mosaic model of the membrane (after Singer [21]).

model Scott and Cheng relate the areas A_i of the projections to those of hard disks and then apply scaled particle theory to the hard disc mixture. More recently Scott [10] models the projections as capped rectangles with the orientations of the particles in the plane of the layer restricted to multiples of 60°. Here we use the capped rectangle with no restriction on the orientation. This means that if the bilayer is viewed from above we see a fluid mixture of capped rectangles (see figure 2(*a*)) in which the length-to-breadth ratio (b/σ) reflects the conformational state of the lipid. In the course of the simulation (b/σ) can change under the influence of neighbouring lipids. In our model the in-plane liquid structure and the conformational disorder of the lipids are coupled.

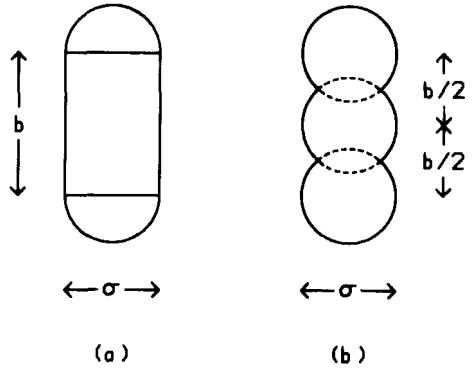

Figure 2. (*a*) The capped rectangle of Scott [10]. (*b*) The triatomic approximation.

We have further simplified the model of Scott and Cheng by replacing the convex capped rectangles (suitable for scaled particle theory) by a triatomic composed of three overlapping discs (see figure 2(*b*)). A dumb-bell would not be suitable for states of the model with $b/\sigma > 1$. An overlap of a pair of these hard triples is more easily identified in the simulation than the overlap of the convex objects. The seven possible states of the lipid and the corresponding geometry of the projections are given in table 1.

Table 1. Properties of the seven-state model for DPPC and the corresponding capped rectangles. $\sigma = 5{\cdot}27$ Å.

State number	ω_i	g_i	A_i/Å^2	b_i/Å^2	b_i/σ
1	1	0	40·8	3·60	0·684
2	24	2	43·5	4·12	0·781
3	280	3·79	46·6	4·70	0·892
4	1328	5·90	50·2	5·39	1·022
5	328	4·78	54·4	6·18	1·173
6	256	4·84	59·3	7·11	1·350
7	24	4·50	65·2	8·23	1·562

3. Computational techniques

3.1. *Constant NVT Monte Carlo*

The standard Metropolis procedure [23] was used for the two-dimensional Monte Carlo simulations. The probability $P(j)$ of a given particle being in bond length state

j is determined by considering the average number of gauche rotations, g_j, and the degeneracy, ω_j, of that state

$$P(j) = \frac{\omega_j \exp[-g_j\varepsilon_g/kT]}{\sum_{i=1}^{m} \omega_i \exp[-g_i\varepsilon_g/kT]}, \quad (1)$$

where ε_g ($= 1{\cdot}68\,\mathrm{kJ\,mol^{-1}}$) is the energy per gauche rotation and k is the Boltzmann constant. Moves are accepted with a probability given by $\min(1, P_{ij})$ where

$$P_{ij} = \frac{\omega_j \exp[-g_j\varepsilon_g/kT]}{\omega_i \exp[-g_i\varepsilon_g/kT]}. \quad (2)$$

A look up-table is constructed for all possible P_{ij} at a given temperature. Particle moves are effected by a uniform random displacement of the centre of mass of the triple and a uniform random change in θ (the in-plane angle). Moves resulting in overlap are rejected. An equal number of conformational changes and particle moves are attempted.

3.2. *Constant NPT Monte Carlo*

For an isothermal–isobaric simulation an additional attempted change in area must be considered. The probability of accepting a random change from state i, at area $A(i)$, to state j, at area $A(j)$, is given by $\min(1, P_{ij})$ where

$$\left.\begin{aligned} P_{ij} &= \exp(-\delta H_{ij}/kT), \\ \delta H_{ij} &= P\Delta A + \Delta E - NkT\ln(A(i)/A(j)). \end{aligned}\right\} \quad (3)$$

Here P is the two-dimensional or lateral pressure. An attempted area change is performed once every cycle.

3.3. *Simulation details*

To set up a low density system it is a simple matter to use a random number generator to pick the coordinates of each molecule in turn. If a molecule overlaps with those already in position then the coordinates are repicked until a random low density configuration is established. With a high density, typical of that found in a liquid, there is little chance of placing all the molecules using this random sequential packing procedure. For single discs in two dimensions this method is limited to packing fractions below 0·55 [24].

Higher density configurations can be obtained by setting the molecules on a regular lattice and then moving them around using the normal Metropolis algorithm until a random configuration is obtained. This Monte Carlo procedure has two problems. An overlap can result when setting up the lattice if the molecules are of very different sizes and the order imposed by the lattice trends to remain in the configuration at high densities.

A particle scaling algorithm can also be used to generate high density configurations. A low density configuration is set up using the random sequential packing procedure. The molecule diameters are increased until two molecules touch. These are then moved apart along the line joining their centres to allow further scaling to take place. A consequence of this method is that once two molecules come into contact with each other they remain in contact. The final configuration thus shows order indicative of an infinitely strong, very short range attractive potential.

Cornell *et al.* [25] have compared configurations of discs at a packing fraction of 0·5 generated by particle scaling, random sequential packing and Monte Carlo procedures. The Monte Carlo procedure is found to be the most suitable for generating configurations which show only mutual volume exclusion effects. None of the procedures, however, are really suited to densities much higher than 0·5, especially if the molecules vary in size.

The procedure used in this work to set up an equilibrated configuration involves particle scaling supplemented by additional Monte Carlo moves. It is described in the Appendix. In the course of the run the maximum displacements Δx_{max}, Δy_{max} and $\Delta\theta_{max}$ were adjusted to maintain an acceptance ratio of 0·5. In the isothermal–isobaric simulations ΔA_{max} is independently adjusted so that half the attempted box moves are accepted.

Equilibration was performed during the scaling phase described in the Appendix and consisted of typically 5000 cycles. The production phase consisted of runs of approximately 10 000 cycles for 100 particle systems and 2000 cycles for 900 particle systems.

Runs were performed on systems of 100, 400 and 900 triples. Differences between 400 and 900 particle runs are within the estimated errors and both sets of results are reported in §4.

4. Results and discussion

4.1. *Introduction*

Figure 3 shows instantaneous configurations from 100 particle runs at 35°C as a function of density. Monitoring of the centre of mass trajectories of the triples shows that the simulations represented by (*a*), (*b*) and (*c*) are in the liquid state; see figure 4 (*a*). In simulation (*d*) the centre of mass trajectories (figure 4 (*b*)) are localized and the hard triples exhibit significant translational ordering. The equilibrium crystal structure of a two-dimensional interaction site model of a polydispersed mixture has not been established but it is almost certainly incommensurate with the square box used in the simulations. For this reason structure (*d*) is best thought of as a metastable glass rather than a true crystalline structure. This freezing we observe is the two-dimensional analogue of the chain melting transition of the lipid bilayer.

Figure 3 suggests that the simulations do not exhibit any long range orientational correlations. It is difficult to draw conclusions from the $N = 100$ system and we investigate this point for $N = 900$ more fully in §4.3. It is clear from the figures that the number of fully extended triples decreases as the density increases. In the remainder of this section we will explore these features of the liquid structure in more detail.

4.2. *Conformation distributions*

In the simulations the final distribution of conformations (bond lengths in the projection) can be calculated as a function of density and temperature. These distributions are shown for the 900-triple simulations in figure 5. The solid line shows the underlying distribution function at 35°C. This is the distribution of states which would be observed at very low density. As the density is increased the distribution tends towards states corresponding to a smaller cross-sectional area. At an area per molecule of approximately 200 Å^2 states 3 and 4 (see the table) are equally probable. At higher densities state 3 is the most probable state despite its lower degeneracy.

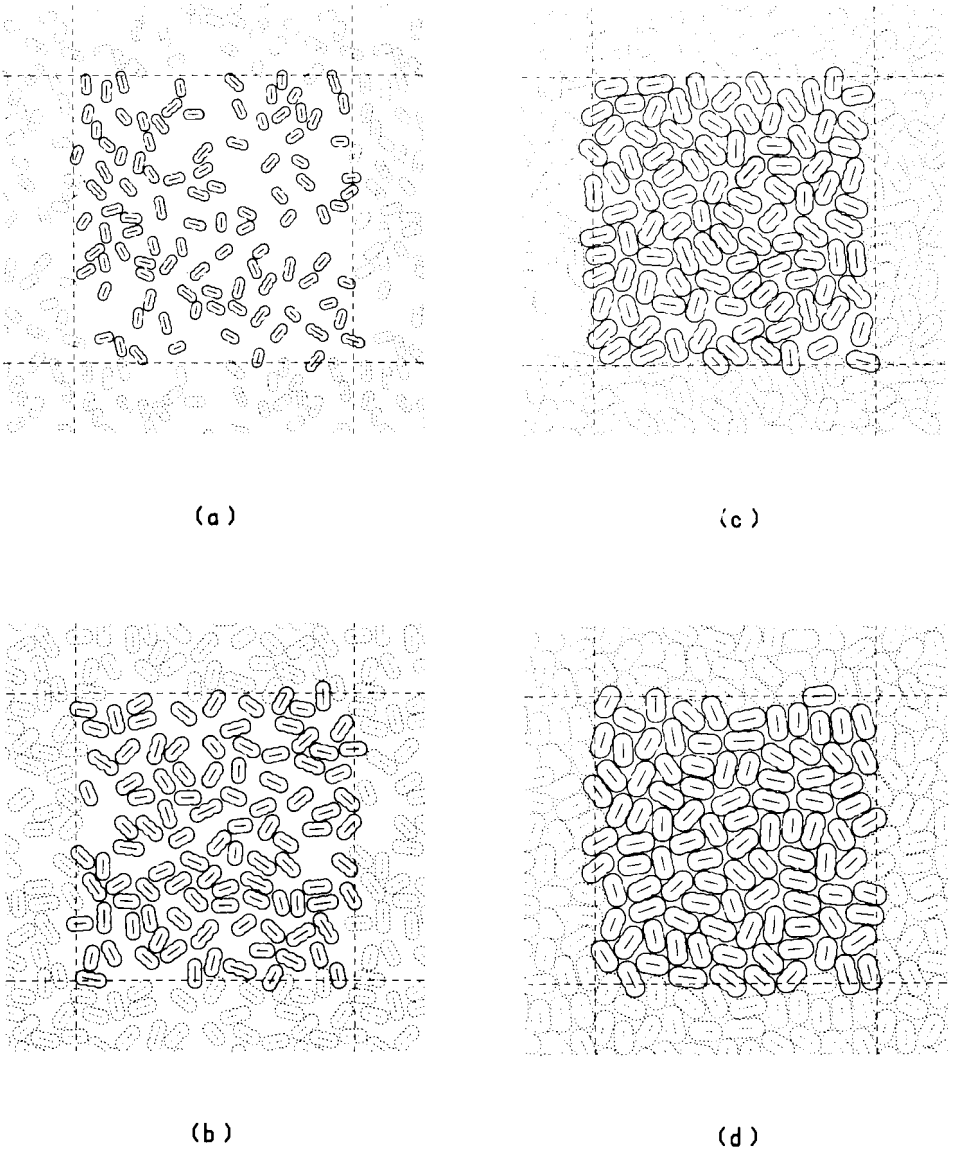

Figure 3. Instantaneous configurations of 100 triples at 35°C at areas per molecule of (*a*) 204·03 Å^2, (*b*) 102·02 Å^2, (*c*) 68·01 Å^2, (*d*) 54·41 Å^2.

At the highest densities, corresponding to the crystalline/glassy state, the most probable bond length state shifts to state 2.

This result is mirrored in figure 6 which shows the average length-to-breadth ratio (b/σ) of the lipid cross-section. The up-triangles are for 100-triple runs, the down-triangles are for 400-triple runs and the crosses, which are coincident with the down-triangles, are for 900-triple runs. The average bond length decreases gradually to a value of 0·85 at an area per molecule of 80 Å^2. There is then a more rapid decrease to 0·77 at 54 Å^2 per molecule. The average number of gauche rotations per molecule (that is twice the number per hydrocarbon chain) is shown in figure 7. This also

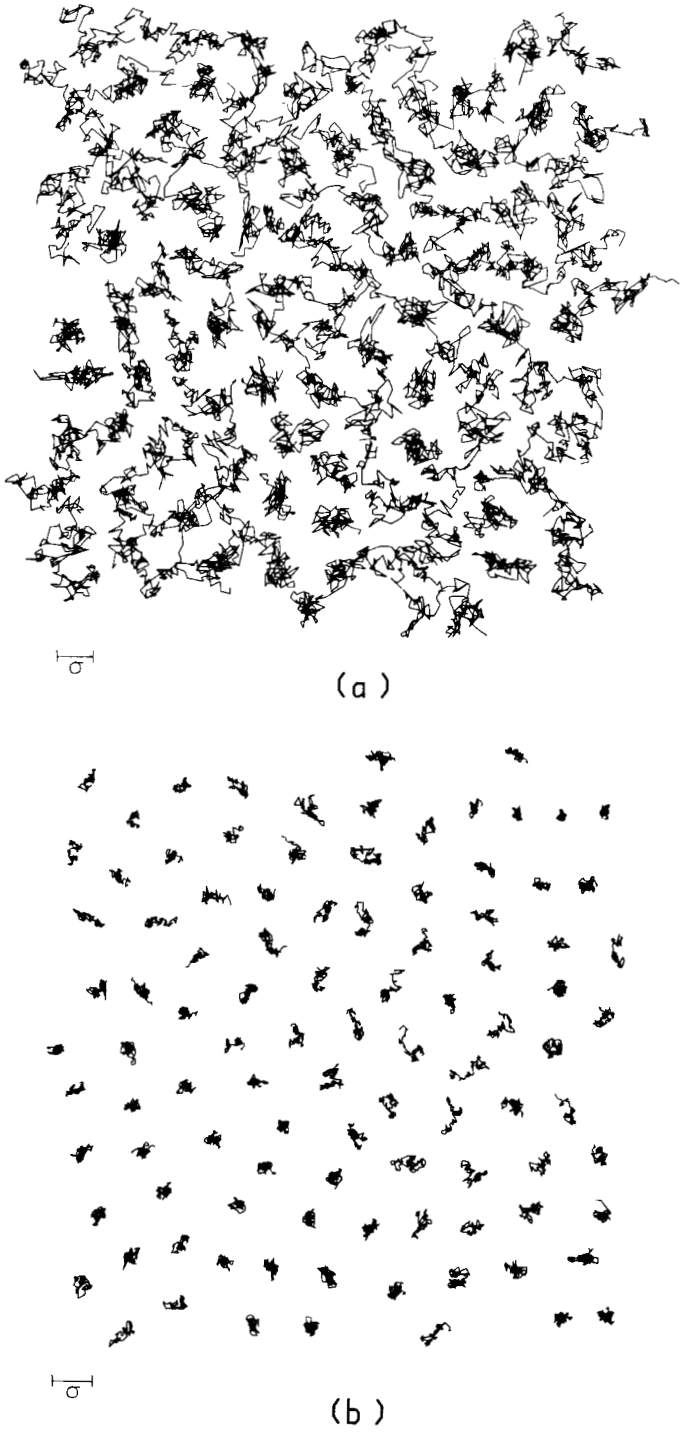

Figure 4. Centre of mass trajectories of 100 triples during runs at 35°C at areas per molecule of (*a*) 68·01 Å^2, (*b*) 54·41 Å^2. The positions are recorded every 50 cycles.

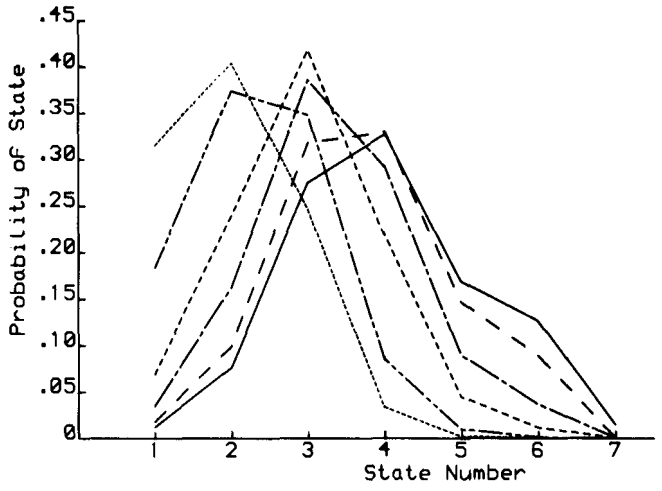

Figure 5. The distributions of bond length states at 35°C for areas per molecule of 204·03 Å^2 (— — —); 102·02 Å^2 (– – –); 68·01 Å^2 (– – – –); 58·29 Å^2 (– · – ·); and 54·41 Å^2 (· · · ·). The solid line represents the underlying distribution at 35°C.

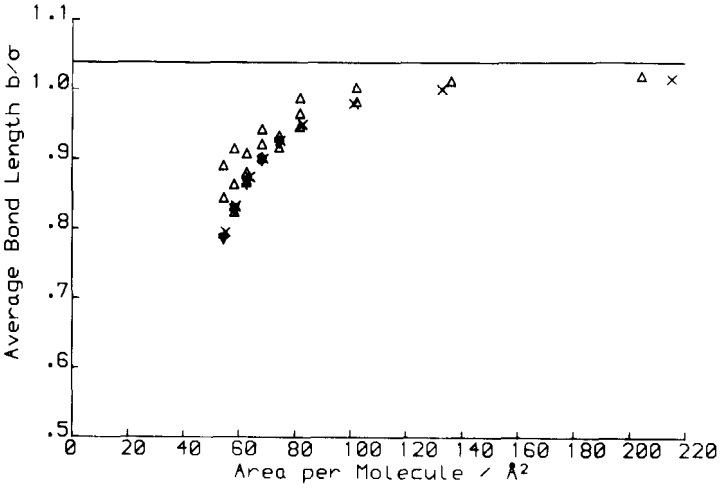

Figure 6. The average bond length as a function of area per molecule at 35°C for constant NVT systems of △, 100 triples; ▽, 400 triples; +, 900 triples, and ×, for constant NPT systems of 100 triples. The solid line shows the average bond length for the underlying distribution at 35°C.

decreases rapidly at areas less than 80 Å^2 to a value of slightly below two at the highest density considered (which might correspond to one all-trans chain and one chain with a g^+tg^- kink). In this model we do not find a discontinuous change, or jump, in either the average bond length or the number of gauche rotations with increasing density in the range studied.

The average length-to-breadth ratio (b/σ) and the number of gauche rotations would be order parameters for the chain melting transition which is first order below a tricritical point [26]. In our case the number of gauche rotations changes continuously even for the 900-triple system. Possible explanations for the lack of a clear

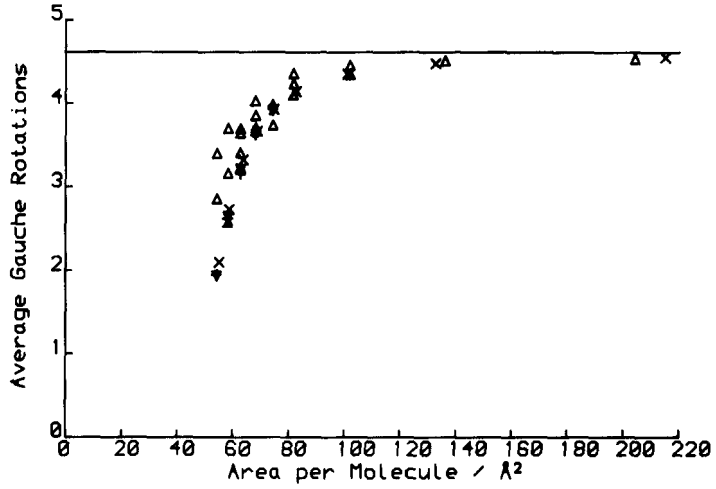

Figure 7. The average number of gauche rotations as a function of area per molecule at 35°C. △, 100 triples; ▽, 400 triples; +, 900 triples; and x, for constant NPT systems of 100 triples. The solid line shows the average number of gauche rotations for the underlying distribution at 35°C.

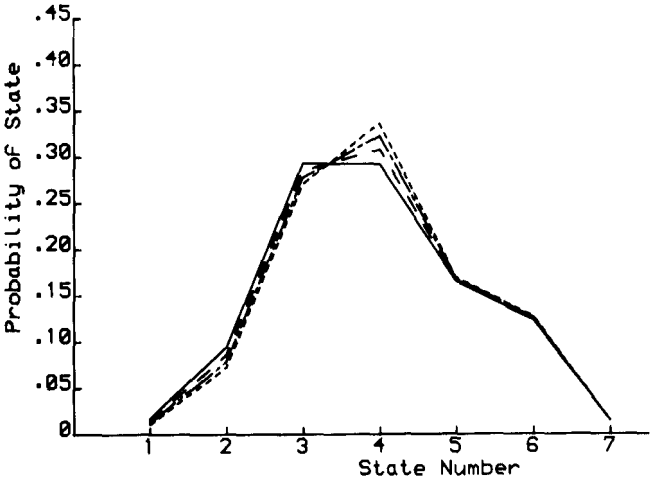

Figure 8. The underlying distributions of bond length states at temperatures of 0°C (——); 15°C (— — —); 30°C (— — —); and 45°C (— — —).

first order phase transition are (1) the absence of attractive forces in our model, which are included in many other models of the liquid-expanded to liquid-condensed transition [6–8, 10–15]; (2) a smearing out of the transition because of the variable bond lengths of the lipids; (3) suppression of the transition by the symmetry of the simulation box.

Figure 8 shows the temperature dependence of the low density distribution of states in the biologically relevant range of 0–45°C. The distribution is almost temperature independent, with a slight shift from state 4 to 3 at the lowest temperatures. At the higher densities considered the distribution is again almost temperature independent, with a slight shift from state 3 to state 2.

4.3. *Liquid structure*

Figure 9 shows the centre–centre pair radial distribution functions with increasing density at 35°C.

$$g(r_{ij}) = N_{av}(r_{ij})/(2\pi\varrho r_{ij}\delta r_{ij}), \tag{4}$$

where $N_{av}(r_{ij})$ is the average number of particles j in a shell of width δr_{ij} at a distance r_{ij} from a particle i. This particular distribution function does not distinguish between the species of triples i and j.

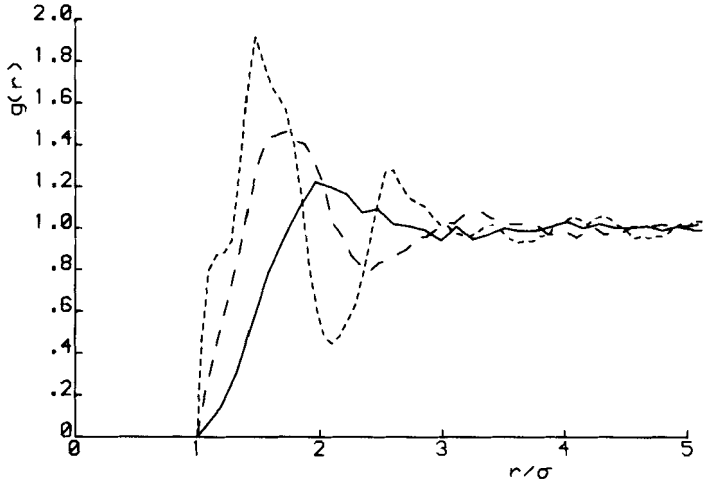

Figure 9. Centre–centre radial distribution functions for systems of 100 triples at 35°C at areas per molecule of 204·03 Å^2 (——); 81·61 Å^2 (— — —); and 58·29 Å^2 (----).

At the lowest density the distribution function resembles the Mayer function exhibiting only a nearest neighbour peak. At an area per molecule of 58·29 Å^2, $g(r)$ has the structure typical of a liquid of hard-core anisotropic particles. The small shoulder at $r/\sigma = 1$ corresponds to parallel configurations, and the main peak can be associated with T configurations of triples in states 2 and 3. The splitting of the first peak is associated with short range orientational order. There is no long range translational order at these densities.

A two-dimensional orientational order parameter for the system, S_2, has been calculated;

$$S_2 = \langle \cos 2[\theta_i - \alpha] \rangle, \tag{5}$$

where θ_i is the angle that triple i makes with a space fixed axis and α is the angle between the director and the same axis. As the triples are linear α is easily determined;

$$\tan(2\alpha) = \frac{\sum_{i=1}^{N} \sin(2\theta_i)}{\sum_{i=1}^{N} \cos(2\theta_i)}. \tag{6}$$

In the absence of long range orientational order in the bilayer plane S_2 should tend to zero and in a perfectly ordered nematic $S_2 = 1$.

A short range order parameter was also calculated to examine the degree of local order within the system. This was based on the definition of the local director $\varphi(\mathbf{r}_j)$ put forward by Frenkel and Eppenga [27].

$$\tan(2\varphi(\mathbf{r}_j)) = \frac{\sum_{i=1}^{N} [\omega(\mathbf{r}_j - \mathbf{r}_i)\sin(2\theta_i)]}{\sum_{i=1}^{N} [\omega(\mathbf{r}_j - \mathbf{r}_i)\cos(2\theta_i)]}, \tag{7}$$

with

$$\left.\begin{aligned} \omega(\mathbf{r}_j - \mathbf{r}_i) &= \exp\left\{-\beta\left[\frac{r_\parallel^2}{\sigma_\parallel^2} + \frac{r_\perp^2}{\sigma_\perp^2}\right]\right\}, \\ S &= \langle\omega(\mathbf{r}_j - \mathbf{r}_i)\cos 2[\theta_i - \varphi(\mathbf{r}_j)]\rangle, \end{aligned}\right\} \tag{8}$$

where $\mathbf{r}_i$ and $\mathbf{r}_j$ are the coordinates of triples i and j, $r_\parallel$ and $r_\perp$ are the components of $(\mathbf{r}_j - \mathbf{r}_i)$ parallel to and perpendicular to the orientation of triple i, $\sigma_\parallel = \sigma_{ij} + (b_i + b_j)/2$ and $\sigma_\perp = \sigma_{ij}$. A β value of 1·65 was chosen to give the order parameter a maximum value of approximately 1. This choice of β gives an effective range of two nearest neighbour shells for the short range order parameter S.

Both S_2 and S were calculated every ten cycles. These order parameters are shown in figure 10 as a function of area per molecule. No long range order develops in these systems either in the liquid state or the crystalline/glassy state. The short range order rises to approximately 0·8 at the highest densities and is continuous across the transition. Our model does not predict a rotor-solid phase similar to that described by Marsh [28]. This can be seen from figure 11 which gives the orientation of the triple axes at intervals of 200 cycles for 140 particles from a 900 particle system. The length of the vectors is equal to the diameter σ. It can be seen that little reorientation takes place over the 1000 cycle span illustrated.

Our system freezes into a glassy structure with the orientation of the long axis of the triple (the short axis of the lipid) fixed. This is almost certainly not the equilibrium

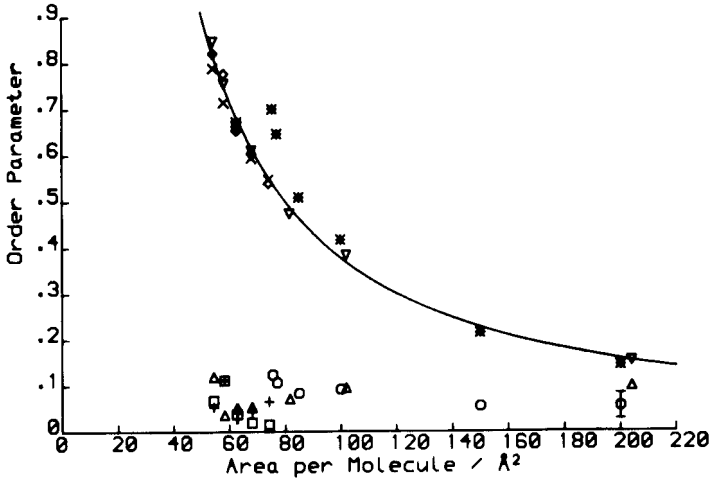

Figure 10. Long and short range order parameters at 35°C for system sizes of △, ▽, 100 triples; +, ×, 400 triples; □, ◇, 900 triples. Order parameters for ○, ∗, the underlying distribution are also shown. The solid line is a guide for the eye only.

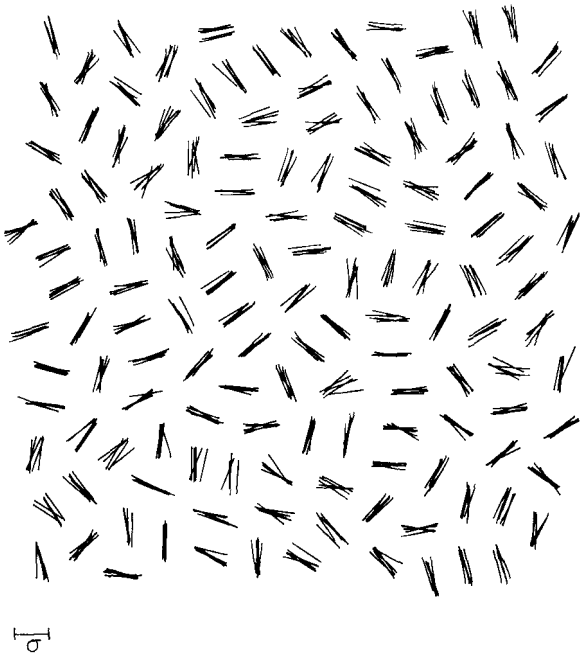

Figure 11. The long axis orientations of 140 triples from a 900 triple system at an area per molecule of 54·41 Å^2. The vectors are each of length σ, centred at the centres of mass. The angles and positions are recorded every 200 cycles.

solid structure for the two-dimensional analogue of the membrane. In a simulation the formation of the equilibrium solid from a fluid by increasing the density is difficult for two reasons. Close to the freezing point the time for the translational and orientational rearrangement required to form the lattice is much longer than even the longest simulation which can be performed in a systematic study of the model. The periodic boundary condition used for the fluid may be incommensurate with the equilibrium solid structure and this will enhance the formation of a glass.

Interestingly, the phase diagrams of the two-dimensional, hard-core triples have not been established even in the case of the one component system where the bond length of the overlapping discs is fixed. In our case where the system is polydispersed an accurate location of the melting transition would require the calculation of the complete chemical potential distribution on both sides of the transition. This is not feasible at present.

Also shown in figure 10 are the long and short range order parameters obtained by fixing the conformational distribution at its low density value. These values are within estimated errors of those obtained using unconstrained systems at areas per molecule greater than about 100 Å^2. At higher densities both the long and short range orientational order are greater than those for the unconstrained systems. The increase is more significant in the case of the short range order. The longer molecules of the constrained system experience greater steric hindrance thus increasing the local orientational order.

4.4. *Thermodynamic properties*

A value for the chemical potential can be obtained using Widom's particle insertion method [29]. If $\delta E_i^{\mathrm{TEST}}$ is the potential energy change which would result

from the random addition of a test triple of species i to the system then the excess chemical potential of species i is

$$\mu_i^{EX} = -kT\ln\langle\exp(-\delta E_i^{TEST}/kT)\rangle. \quad (9)$$

For hard-core particles $\langle\exp(-\delta E_i^{TEST}/kT)\rangle$ is the average probability, $\langle P_i^{Acc}\rangle$, of a successful insertion of a test particle.

A lattice of 25 particles of a particular bond length each at an angle of 45° to a space fixed axes is inserted into the fluid at intervals of 10 cycles. The species on the lattice is replaced with a species of a different bond length and the process is repeated to give a chemical potential distribution at each density. The results are shown in figure 12 and are given in table 2. The chemical potential distribution across the states is almost uniform at each density.

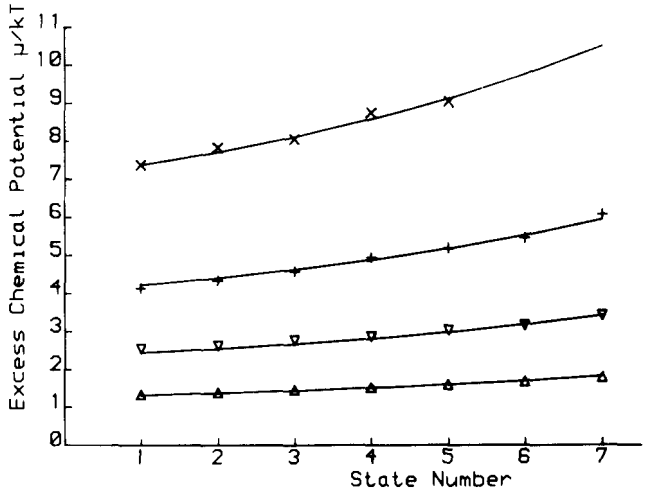

Figure 12. The reduced excess chemical potential for systems of 100 triples at 35°C at areas per molecule of △, 204·03 Å^2; ▽, 136·02 Å^2; +, 102·02 Å^2; and x, 81·61 Å^2. The solid lines give the excess chemical potential obtained using scaled particle theory (equation (10)) for the same densities.

Table 2. Typical values of reduced excess chemical potential, μ^{EX}/kT, at the given area per molecule for each state. WPI denotes simulation data using Widom's particle insertion method. SPT indicates data obtained from equation (10).

State number	204 Å^2		136 Å^2		102 Å^2		82 Å^2	
	WPI	SPT	WPI	SPT	WPI	SPT	WPI	SPT
1	1·34	1·32	2·54	2·44	4·12	4·21	7·49	7·35
2	1·39	1·38	2·62	2·54	4·33	4·40	7·82	7·71
3	1·46	1·44	2·76	2·66	4·57	4·62	8·05	8·10
4	1·52	1·51	2·87	2·81	4·93	4·87	8·74	8·57
5	1·59	1·60	3·03	2·97	5·17	5·17	9·03	9·11
6	1·68	1·70	3·14	3·17	5·45	5·52	–	9·74
7	1·79	1·83	3·40	3·41	6·07	5·95	–	10·50

A value for the chemical potential distribution of the system can be calculated using scaled particle theory [30, 31]. Thus

$$\frac{\mu_i}{kT} = \ln \Lambda_i \varrho_i - \ln(1 - \Sigma \varrho_j A_j) + \frac{A_i \Sigma \varrho_j + s_i \Sigma \varrho_j s_j / 2\pi}{1 - \Sigma \varrho_j A_j} + \frac{A_i (\Sigma \varrho_j s_j)^2}{4\pi (1 - \Sigma \varrho_j A_j)^2}, \quad (10)$$

where ϱ_i are the number densities, A_i are the areas of the molecules and s_i are the perimeter lengths of the molecules. The summations are over the species and

$$\Lambda = h^2/(2\pi mkT)h/\sqrt{(8\pi^2 IkT)}$$

is the ideal gas partition function for a plane rigid rotor.

The number densities ϱ_j, corresponding to the final distribution of states, were obtained by calculating the average number of triples in each state over the whole simulation. Although the Monte Carlo calculations were carried out using triples, which are clearly not convex molecules it is reasonable to assume that a fluid of the equivalent capped rectangles will have similar properties to a fluid of triples. The values of A_i and s_i used correspond to the capped rectangles. The use of the real A_i and s_i for the triple lowers the estimated chemical potential distribution by 0·05 per cent. The agreement between equation (10), shown as solid lines in figure 12, and the simulation results is excellent at areas per molecule of 204 Å^2, 136 Å^2 and 102 Å^2. At 82 Å^2 reasonable estimates for the chemical potential from the simulation are obtained for states 1 to 5 but the Widom insertion technique fails completely for the molecules with longer bond lengths since there are no successful insertions. Even under these circumstances the scaled particle theory fits the available points and is a useful functional form for extrapolating to regions where the Widom method fails.

The pressure for a fluid of triples can be calculated from a knowledge of the site–site distribution functions ($g_{00}(r_{\alpha\gamma})$) and their first circular harmonics ($g_{10}(r_{\alpha\gamma})$) in the site–site frame at contact ($r_{\alpha\gamma} = \sigma$) [32]. There are 3 independent site–site distributions per pair of triples and 28 different pairs of triples in the 7 state model. The extrapolation of 84 functions to contact and the subsequent accumulation of errors makes this an unreasonable route to the pressure. To calculate pressures for this model we switch to the constant NPT ensemble. Here the pressure is fixed and the area per molecule calculated as an ensemble average. We have checked that results for quantities such as the short range order parameter are independent of our choice of ensemble. The results for the equation of state are shown in figure 13 and are given in table 3. The down-triangles are the constant NPT simulation results. The up-triangles are the scaled particle theory results for the equation of state

$$\frac{P}{kT} = \frac{\Sigma \varrho_i}{1 - \Sigma \varrho_i A_i} + \frac{(\Sigma \varrho_i s_i)^2}{4\pi (1 - \Sigma \varrho_i A_i)^2}. \quad (11)$$

Considering the uncertainties in the ϱ_i obtained in the NVT simulations the agreement between this theory and the exact result is excellent. Also shown as a line in figure 13 is the scaled particle theory equation of state obtained from the low density distribution of conformational states. The ability of the triples to change their length under the influence of their neighbours reduces the pressure at a particular area per molecule.

We stress that equation (11) is not an *a priori* theory for the pressure; it requires a knowledge of the final distribution of states from the simulation. Figure 14 shows the simulation pressures plotted against packing fraction and the scaled particle

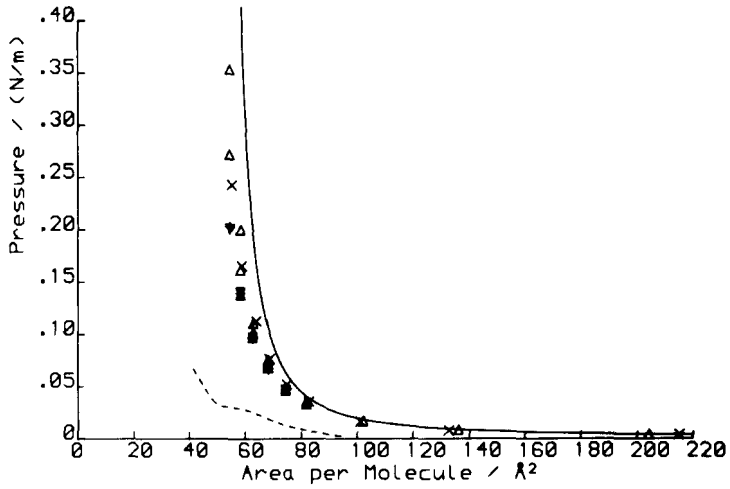

Figure 13. Lateral pressure as a function of area per molecule at 35°C. Data from constant NVT simulations using scaled particle theory (equation (11)) for system sizes of △, 100 triples; ▽, 400 triples; +, 900 triples; and x, data from constant NPT simulations for 100 triple systems. The isotherm for the underlying distribution at 35°C (——); and experimental data at 34·1°C [33] (----); are also shown.

Table 3. Typical values of the area per molecule, the lateral pressure and the order parameters for the NVT and NPT systems respectively.

NVT					NPT				
Area per molecule /Å^2	Packing fraction	SPT pressure /mN m^{-1}	S_2	S	Pressure /mN m^{-1}	Average area per molecule /Å^2	Packing fraction	S_2	S
204·03	0·24	3·8	0·10	0·15	3·47	214·8	0·21	0·09	0·12
136·02	0·35	8·3	0·09	0·22	7·52	132·6	0·37	0·10	0·24
102·02	0·47	16·5	0·09	0·38	16·27	101·0	0·49	0·09	0·34
81·61	0·57	34·0	0·07	0·47	35·21	82·6	0·58	0·10	0·47
74·19	0·63	47·7	0·05	0·54	51·80	74·7	0·62	0·06	0·54
68·01	0·68	71·3	0·04	0·60	76·19	68·6	0·69	0·08	0·58
62·78	0·71	111·	0·04	0·66	112·1	63·9	0·71	0·08	0·69
58·29	0·76	161·	0·09	0·74	164·9	58·8	0·76	0·07	0·75
54·41	0·79	272·	0·06	0·83	242·5	55·2	0·79	0·11	0·83

theory results for the *low density* (*underlying*) distribution at the same packing fractions. The agreement is good. This indicates that we do not require the complete distribution of states to estimate the pressure. A knowledge of the first moment of this distribution determines the packing fraction and from figure 14 a reasonable estimate of P.

5. Conclusions

We have shown that the conformational distribution of the hydrocarbon chains in a model of the lipid bilayer is significantly affected by changes in the lipid density. At 35°C the average length-to-breadth ratio (b/σ) of the lipid cross-section changes

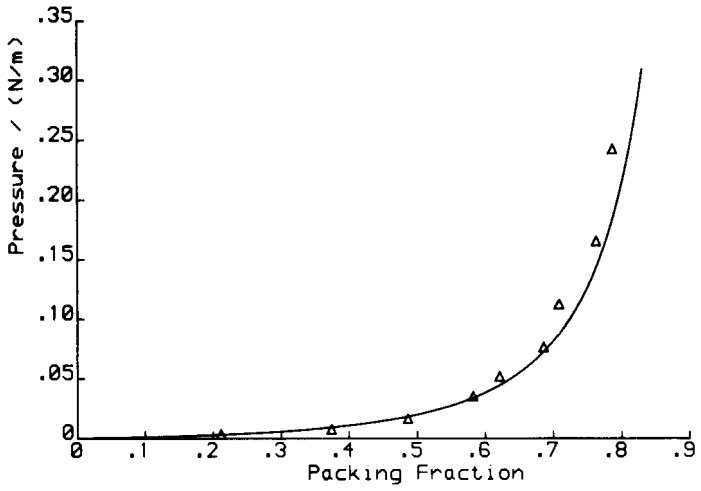

Figure 14. Lateral pressure as a function of packing fraction at 35°C from constant NPT simulations △ for 100 triple systems. The solid line gives the pressure for the underlying distribution at 35°C.

from 1·02 to 0·77 as the area per head group changes from 204 Å^2 to 54 Å^2. At the same time a change of temperature over the biologically relevant range of 0–45°C scarcely alters the average cross-section of the molecules. The number of gauche rotations per lipid molecule decreases continuously to an average value of 2 at approximately 54 Å^2 per molecule. In our model these changes are induced simply by excluded volume interactions between the lipids. We speculate that similar results will be seen when normal inter-chain dispersion interactions are introduced into the model. In this case we might expect an initial small extension of the lipids with increasing density before they contract.

Our system appears to freeze between packing fractions of $\eta = 0{\cdot}71$ and $\eta = 0{\cdot}76$. This compares with the freezing packing fraction for hard discs of $\eta_{\text{liquid}} = 0{\cdot}68$ and $\eta_{\text{solid}} = 0{\cdot}72$ [34]. The number of gauche rotations per molecule and the pressure in this region are continuous functions of packing fraction suggesting a continuous transition. Since the two-dimensional hard disc transition is a firmly established first order transition, a possible explanation would be that the variability in the bond lengths of the triples broadens the transition, washing out its first order character. We stress that we are unable to make a firm conclusion from our studies because of the effects of the boundary conditions on the transition. A possible way of resolving this problem would be to set up a rectangular cell of translationally ordered triples and to perform a series of runs at decreasing density. Even in this case we may need to constrain molecules to smaller cells to avoid two-phase behaviour in the simulation and to construct the Van der Waals loop for the transition [35]. The number of configurational states used in the model may also affect the packing of the triples around the phase transition. Although seven states are certainly fewer than the 21 states originally used by Scott in an earlier model [36], similar two and ten state models of the lipid bilayer used extensively by Pink and co-workers have proved to be very successful. These have been reviewed by Mouritsen [37] who looks at the effect of the number of states q upon the average area per molecule as a function of temperature across the transition. Hysteresis behaviour, present for values of $q \leqslant 5$,

disappears for $q \geqslant 6$ giving a continuous transition, as found in experimental studies of lipid bilayers. It seems reasonable, therefore, that the simpler seven state model is sufficient in this study.

The P–A isotherm obtained using scaled particle theory is in excellent agreement with the constant NPT simulation results. The lateral pressure is reduced by allowing the bond lengths of the triples to vary from the underlying distribution of bond lengths. Interestingly, despite the crude nature of the model, the isotherm is within an order of magnitude of experimental isotherms (see figure 13).

We plan to extend this work in two directions by including attractive forces in the two-dimensional analogue, and by including larger protein discs in the simulation.

We would like to thank the SERC for a generous grant of computer time.

Appendix

The state of each triple was first chosen at random, subject to the probability distribution given by equation (1). A random system was then set up using the following method.

Configurations of particles were established as follows:

(i) set up a low density system using a random sequential packing procedure;

(ii) scale the system down until two molecules touch;

(iii) perform ten Monte Carlo cycles;

(iv) repeat (ii) and (iii) until the required density is obtained.

Scaling the cell size and molecule coordinates, rather than the molecular diameters, reduces cumulative rounding errors.

A point $\mathbf{p}$ is chosen arbitrarily and the centre of mass coordinates $\mathbf{q}$ of the molecules are scaled towards P by a factor S. The new coordinates $\mathbf{f}(\mathbf{q})$ are given by

$$\mathbf{f}(\mathbf{q}) = \mathbf{p} + S(\mathbf{q} - \mathbf{p}), \tag{A 1}$$

$$\mathbf{f}(\mathbf{q}) - \mathbf{f}(\mathbf{r}) = S(\mathbf{q} - \mathbf{r}). \tag{A 2}$$

All choices of $\mathbf{p}$ are equivalent for the purpose of scaling the configuration and it is convenient to chose the origin.

A pair of molecules i, j will touch when

$$|\mathbf{f}(\mathbf{q}_i) - \mathbf{f}(\mathbf{q}_j)| = \sigma_{ij}. \tag{A 3}$$

The scale factor for a particular pair, S_{ij}, is given by

$$S_{ij} = \sigma_{ij}/|\mathbf{q}_i - \mathbf{q}_j|. \tag{A 4}$$

For a system containing more than two molecules all the S_{ij}s are computed and the largest, $S_{\max}$, is selected. Then

$$\mathbf{f}(\mathbf{q}) = S_{\max}\mathbf{q}. \tag{A 5}$$

The method can be extended to a composite hard-core molecule made up from a set of hard discs or spheres. Each molecule is described by its centre of mass coordinates $\mathbf{q}$ and the vectors $\mathbf{l}_\alpha$ from its centre of mass to each site α in the molecule.

Consider the αth site of molecule i and the βth site of molecule j. The scaling factor $S_{i\alpha j\beta}$ is calculated for each site–site separation and is given by

$$S_{i\alpha j\beta} = [-\mathbf{Q}_{ij}.\mathbf{L}_{\alpha\beta} \pm ([\mathbf{Q}_{ij}.\mathbf{L}_{\alpha\beta}]^2 - \mathbf{Q}_{ij}^2\mathbf{L}_{\alpha\beta}^2 + \mathbf{Q}_{ij}^2\sigma_{ij}^2)^{1/2}]/\mathbf{Q}_{ij}^2, \quad \text{(A 6)}$$

with

$$\left.\begin{aligned}\mathbf{Q}_{ij} &= \mathbf{g}_i - \mathbf{g}_j,\\ \mathbf{L}_{\alpha\beta} &= \mathbf{l}_{i\alpha} - \mathbf{l}_{j\beta}.\end{aligned}\right\} \quad \text{(A 7)}$$

$S_{\max} = \max(S_{i\alpha j\beta})$ and $\mathbf{f}(\mathbf{q})$ is calculated from equation (A 5).
$([\mathbf{Q}_{ij}.\mathbf{L}_{\alpha\beta}]^2 - \mathbf{Q}_{ij}^2\mathbf{L}_{\alpha\beta}^2 + \mathbf{Q}_{ij}^2\sigma_{ij}^2)$ may become negative if either $|\mathbf{l}_{i\alpha}| > \sigma_i/2$ or $|\mathbf{l}_{j\beta}| > \sigma_j/2$. In this situation $S_{i\alpha j\beta}$ can be set to zero without affecting the scaling. This technique applies equally to soft potentials where σ_{ij} is defined by

$$u_{ij}(\sigma_{ij}) = 0. \quad \text{(A 8)}$$

References

[1] Petrov, A. G., Seleznev, S. A., and Derzhanski, A., 1979, *Acta phys. pol.*, **55**, 385.
[2] Hauser, H., Pascher, I., Pearson, R. H., and Sundell, S., 1981, *Biochim. biophys. Acta*, **650**, 21.
[3] Scott, H. L., 1984, *Comments molec. cell. Biophys.*, **2**, 197.
[4] Seelig, J., and Seelig, A., 1980, *Q. Rev. Biophys.*, **13**, 19.
[5] See, for example, Lee, A. G., 1975, *Prog. Biophys. molec. Biol.*, **29**, 5 and references therein.
[6] Scott, H. L., Jr., and Cheng, W. H., 1977, *J. Colloid Interface Sci.*, **62**, 125.
[7] Scott, H. L., and Cheng, W. H., 1979, *Biophys. J.*, **28**, 117.
[8] Pink, D. A., Georgallas, A., and Zuckermann, M. J., 1980, *Z. Phys.* B, **40**, 103.
[9] Zuckermann, M. J., and Pink, D., 1980, *J. chem. Phys.*, **73**, 2919.
[10] Scott, H. L., 1981, *Biochim. biophys. Acta*, **643**, 161.
[11] Zuckermann, M. J., Pink, D. A., Costas, M., and Sanctuary, B. C., 1982, *J. chem. Phys.*, **76**, 4206.
[12] Georgallas, A., and Pink, D. A., 1982, *J. Colloid Interf. Sci.*, **89**, 107.
[13] Mouritsen, O. G., Boothroyd, A., Harris, R., Jan, N., Lookman, T., MacDonald, L., Pink, D. A., and Zuckermann, M. J., 1983, *J. chem. Phys.*, **79**, 2027.
[14] Kambara, T., and Sasaki, N., 1984, *Biophys. J.*, **46**, 371.
[15] Marčelja, S., 1974, *Biochim. biophys. Acta*, **367**, 165.
[16] Gruen, D. W. R., 1980, *Biochim. biophys. Acta*, **595**, 161.
[17] Khalatur, P. G., 1982, *Polymer Sci. USSR*, **24**, 2356.
[18] Busico, V., and Vacatello, M., 1983, *Molec. Crystals liq. Crystals*, **97**, 195.
[19] van der Ploeg, P., and Berendsen, H. J. C., 1983, *Molec. Phys.*, **49**, 233.
[20] Werge, C., and Binder, H., 1983, *Studia Biophysica*, **93**, 219.
[21] Singer, S. J., and Nicolson, G. L., 1972, *Science, N.Y.*, **175**, 720.
[22] Kuo, A. L., and Wade, C. G., 1979, *Biochemistry*, **18**, 2300.
[23] Metropolis, N., Rosenbluth, A. W., Rosenbluth, M. N., Teller, A. H., and Teller, E., 1953, *J. chem. Phys.*, **21**, 1087.
[24] Tanemura, M., 1979, *Ann. Inst. statist. Math.*, **31**, 351.
[25] Cornell, B. A., Middlehurst, J., and Parker, N. S., 1981, *J. Colloid Interface Sci.*, **81**, 280.
[26] Nagle, J. F., 1986, *Faraday Discuss. chem. Soc.*, **81**, 151.
[27] Frenkel, D., and Eppenga, R., 1985, *Phys. Rev.* A, **31**, 1776.
[28] Marsh, D., 1980, *Biochemistry*, **19**, 1632.
[29] Widom, B., 1963, *J. chem. Phys.*, **39**, 2808.
[30] Boublik, T., 1975, *Molec. Phys.*, **29**, 429.
[31] Talbot, J., 1985, Ph.D. thesis, Southampton University.

[32] LAJTAR, L., PENAR, J., and SOKOLOWSKI, S., 1987, *J. chem. Soc. Faraday Trans. I*, **83**, 1405.
[33] See, for example, ALBRECHT, O., GRULER, H., and SACKMANN, E., 1978, *J. Phys., Paris*, **39**, 301.
[34] ALDER, B. J., and WAINWRIGHT, T. E., 1962, *Phys. Rev.*, **127**, 359.
[35] DA SILVA, M. A. A., CALIRI, A., and MOKROSS, B. J., 1987, *Phys. Rev. Lett.*, **58**, 2312.
[36] SCOTT, H. L., JR., 1975, *Biochim. biophys. Acta*, **406**, 329.
[37] MOURITSEN, O. G., 1984, *Computer Studies of Phase Transitions and Critical Phenomena* (Springer Series in Computational Physics) (Springer-Verlag) p. 113.